Pre-impact mutual orbit of the DART target binary asteroid (65803) Didymos derived from observations of mutual events in 2003–2021

P. Scheirich [a,*], P. Pravec [a],

[a] *Astronomical Institute of the Czech Academy of Sciences, Fričova 1, CZ-25165 Ondřejov, Czech Republic*

Preprint submitted to Elsevier Preprint *16 December 2021*

Proposed running head: Didymos mutual orbit modeling

Editorial correspondence to:
Peter Scheirich, Ph.D.
Astronomical Institute AS CR
Fričova 1
Ondřejov
CZ-25165
Czech Republic
Phone: 00420-323-620115
Fax: 00420-323-620263
E-mail address: petr.scheirich@gmail.com

Abstract

We modeled photometric observations of mutual events (eclipses and occultations) between the components of the binary near-Earth asteroid (65803) Didymos, target of the Double Asteroid Redirection Test (DART) space mission, that were taken from 2003 to 2021 (Pravec et al. 2022, submitted). We derived parameters of the modified Keplerian mutual orbit (allowing for a quadratic drift in the mean anomaly, presumably caused by the BYORP effect) of the secondary, called Dimorphos, around the Didymos primary and estimated its diameter. The J2000 ecliptic longitude and latitude of the orbital pole are $320.6^\circ \pm 13.7^\circ$ and $-78.6^\circ \pm 1.8^\circ$, respectively, and the orbital period is 11.921624 ± 0.000018 h at epoch JD 2455873.0 (asterocentric UTC; all quoted uncertainties correspond to 3σ). We obtained the quadratic drift of the mean anomaly of 0.15 ± 0.14 deg/yr^2. The orbital eccentricity is ≤ 0.03. We determined the ecliptic longitude and latitude of the radius vector of Dimorphos with respect to Didymos at the nominal time of the DART impact to Dimorphos (JD 2459849.46875 geocentric UTC) to be $222.8^\circ \pm 7.0^\circ$ and $-1.6^\circ \pm 4.2^\circ$, respectively.

Key words: Asteroids, satellites; Photometry; DART space mission; Hera space mission

* Corresponding author. Fax: +420 323 620263.

Email address: petr.scheirich@gmail.com (P. Scheirich).

1 Introduction

The near-Earth asteroid (65803) Didymos, originally designated 1996 GT, was discovered by the *Spacewatch* asteroid survey from Kitt Peak Observatory in Arizona on 1996 April 11. Its binary nature was revealed by Pravec et al. (2003). Pravec et al. (2006) and Scheirich and Pravec (2009) analyzed and modeled photometric data obtained during its close approach to Earth in 2003. They reported initial estimates of the binary system properties, including parameters of the mutual orbit of the two components. The system was also observed using radar from Arecibo and Goldstone in 2003. The radar observations were published and modeled together with the photometric data by Naidu et al. (2020) who obtained a shape model of the primary and determined or constrained several parameters of the binary asteroid system.

Didymos is classified as an S-type asteroid (Cheng et al., 2018) based on vis-IR spectra obtained by de León et al. (2010), also confirmed by Dunn et al. (2013).

The secondary of the Didymos binary system, recently named Dimorphos, has been selected as a target of the Double Asteroid Redirection Test (DART). It is NASA's first planetary defense test mission, demonstrating the kinetic impactor mitigation technique. It was launched in November 2021, and it will arrive to the Didymos system on the 26th September 2022 at 23:15 UTC and impact into Dimorphos. The main benefit of using a binary asteroid system for a kinetic impactor mission is that it allows the results of the test to be measured from Earth via photometric observations, assuming that the binary system exhibits mutual events seen from Earth. Rivkin et al. (2021) discuss the factors that led to the recognition that Didymos was the best candidate for a kinetic impactor test, and its selection as the DART target system. Several years after the DART impact the Didymos system will be visited by ESA's Hera mission that will provide a thorough description of the post-impact state of the binary system (Michel et al., 2022).

An important part of the preparation of the DART mission has been an observational effort to precisely determine the orbit of the secondary around the primary. For that, Pravec et al. (2022) obtained photometric observations of Didymos system taken with several large- or medium-sized groundbased telescopes from 2015 to 2021. In this paper, we present results from mutual orbit modeling using the complete photometry data for mutual events in the Didymos system from 2003 to 2021. An independent derivation of the mutual orbit based on analysis of mutual event timings has been made by Naidu et al. (in preparation).

2 Mutual orbit model of Didymos system

2.1 Observational data

The data used in our analysis, obtained during five apparitions of Didymos from 2003 to 2021, were published in Pravec et al. (2006, 2022). We briefly summarize them in Table 1. Each row in the table represents one apparition, identified with the mid-UTC date of its first and its last observing session (run) rounded to the nearest tenth of a day in the first column. Subsequent columns give the number of observing runs (labeled as *No. of nights*, but we note that they were taken using several telescopes and so more than one run were sometimes taken on a single night) in the given apparition and a reference to where more information on the observations is available.

The data were analysed using the standard technique described in Pravec et al. (2006, 2022). Briefly, by fitting a two-period Fourier series to data points taken outside mutual (occultation or eclipse) events, the rotational lightcurves of the primary (short-period) and the secondary (long-period), which are additive in flux units, were separated. The long-period (orbital) lightcurve component containing the mutual events and the secondary rotation lightcurve is then used for subsequent numerical modeling. We refer the reader to Pravec et al. (2022) for details of the lightcurve decomposition method.

Table 1
Photometric observations of the Didymos system

Time span	No. of nights	Reference
2003-11-20.9 to 2003-12-20.3	17	P06
2015-04-13.3 to 2015-04-14.4	2	P22
2017-02-23.3 to 2017-05-04.3	13	P22
2019-01-31.4 to 2019-03-11.1	5	P22
2020-12-12.6 to 2021-03-06.3	15	P22

References: P06 (Pravec et al., 2006), P22 (Pravec et al., 2022)

2.2 Numerical model

We constructed the model of the Didymos system using the technique of Scheirich and Pravec (2009) that was further developed in Scheirich et al. (2015, 2021). In the following, we outline the basic points of the method, but we refer the reader to the 2009, 2015, and 2021 papers for details of the technique.

The binary asteroid components were represented with spheres or oblate (for the primary) and prolate (for the secondary) ellipsoids (the ellipsoidal shapes were used to check the sensitivity of the solution to the shapes of the components, see below), orbiting each other on a circular orbit. We choose the circular orbit for simplicity,

as the upper limit on the eccentricity is low (see below). The motion was assumed to be Keplerian, but we allowed for a quadratic drift in the mean anomaly. The spin axis of the primary was assumed to be normal to the mutual orbital plane of the components (i.e., we assumed zero inclination of the mutual orbit). When the secondary was modeled as the prolate spheroid, its long axis was kept aligned with the centers of the two bodies (i.e., in synchronous rotation with zero libration). The shapes were approximated with 1016 and 252 triangular facets for the primary and the secondary, respectively. The components were assumed to have the same albedo. The brightness of the system as seen by the observer was computed as a sum of contributions from all visible facets using a ray-tracing code that checks which facets are occulted by or are in shadow from the other body. A combination of Lommel-Seeliger and Lambert scattering laws was used (see, e.g., Kaasalainen et al., 2002).

The quadratic drift in mean anomaly, ΔM_d, was fitted as an independent parameter. It is the coefficient in the second term of the expansion of the time-variable mean anomaly:

$$M(t) = M(t_0) + n(t - t_0) + \Delta M_d (t - t_0)^2, \tag{1}$$

where

$$\Delta M_d = \frac{1}{2}\dot{n}, \tag{2}$$

where n is the mean motion, t is the time, and t_0 is the epoch. ΔM_d was stepped from -10 to $+10$ deg/yr^2 with a step of 0.01 deg/yr^2, and all other parameters were fitted at each step.

Since the 3-σ upper limit on the eccentricity of the mutual orbit is 0.03 only (Scheirich and Pravec, 2009), we set the eccentricity equal to zero for simplicity and efficiency. This assumption had a negligible effect on the accuracy of other derived parameters of the models. Scheirich and Pravec (2009) estimated the upper limit on the eccentricity using data from the 2003 apparition. We checked that their upper limit is consistent with the data taken in later apparitions, but those data do not possess characteristics necessary to use them for constraining the eccentricity more. Those characteristics include sufficient quality, sufficient time coverage, and/or sufficient depths of the mutual events. Thus, the constraint on the eccentricity by Scheirich and Pravec (2009) still applies.

Except for the data quality, constraining the eccentricity is also hampered by some systematic time offsets of mutual event branches caused by model simplification of the shape of the primary (see below and Fig. 7). A non-zero eccentricity would cause time offsets of the event branches with respect to the solution with circular orbit. For eccentricity of 0.03, these offsets would be up to 5 minutes (corresponding to 2.5° in the mean anomaly of the secondary) for the events occuring close to primary's equator and of up to 8 minutes (5°) duration for the events occuring close to the primary's pole. The magnitude of such offsets is comparable with the magnitude of the offsets caused by the model simplification. Given the presence

of the systematics in the event timings modeling, we therefore do not expect the eccentricity to be constrained more by data from future apparitions.

Across all observations, we found a unique solution for the system parameters, see Table 2. We describe and discuss these parameters in Section 3.

We estimated uncertainties of the fitted parameters using two techniques: the uncertainties of the relative semimajor axis and the orbital pole (these parameters are strongly determined by shapes of the mutual events) were estimated using the procedure described in Scheirich and Pravec (2009). The uncertainties of the rest of the parameters, which are determined primarily by the timings of the events, were estimated using the method described in Scheirich et al. (2021), which we outline below.

The residuals of the model fitted to the observational data do not obey the Gaussian statistics because of systematic errors resulting from model simplifications. In particular, the residuals of nearby measurements appear correlated. To eliminate the effect we adopted the following strategy based on the χ^2 test.

We choose a correlation time d and for each data point (i) we calculated how many other data points, K_i, are within $\pm d/2$ from the given point. We then applied a weight of $1/K_i$ to the given data point in the χ^2 sum. We also calculated an effective number of data points as $N_{\rm eff} = \sum_{i=1}^{N} 1/K_i$, where N is the total number of data points. For normalized χ^2 we then have $\chi^2 = 1/(N_{\rm eff} - M) \sum_{i=1}^{N} (O-C)_i^2/(\sigma_i^2 K_i)$, where M is the number of fitted parameters of the model and σ_i is a standard deviation of the ith point. As the residuals are predominated by model rather than observational uncertainties, we assign each data points the same standard deviation $\sigma_i = \sigma$, where σ is the RMS residual (root mean square of observed magnitudes, O, minus the values calculated from the model, C) of the best fit solution.

The procedure described above is equivalent to reducing the number of data points to one in each time interval with the length d (i.e., to reducing the total number of points to $N_{\rm eff}$) and assigning $(O-C)^2$ of this point to be a mean of $(O_i - C_i)^2$ of all the points within the interval. However, our approach has the advantage that it does not depend on a particular realization of dividing the observing time span into the intervals of length d.

We choose the correlation time d to be equal to 1/2 of the mean duration of a descending/ascending branch of the secondary mutual event, i.e., the mean time between the first and the second or between the third and the fourth contact. For the observed events in Didymos, it is $d = 0.14$ h. (We also tested d to be twice as long, i.e., equal to the full mean duration of the secondary event branch, but we found it to be inadequate as the longer correlation time resulted in a substantial loss of information by deweighting the datapoints too much.)

We note that the mutual orbit model fit is sensitive only to data points covering mutual events and their closest neighborhood. Therefore we limited the above analysis only to such data points; points further outside the events were not used, because they do not effectively contribute to the determination of the mutual orbit.

Upon stepping a given parameter on a suitable interval (while the other parameters fitted) and computing the normalized χ^2 for each step, we determined 3-σ uncertainty of the given parameter as an interval in which χ^2 is below the p-value of the χ^2 test, corresponding to the probability that the χ^2 exceeds a particular value only by chance equal to 0.27%.

Plot of the normalized χ^2 vs ΔM_d is shown in Fig. 1. In order to save computing time, the plots were constructed using spherical shapes for both components. However, a neighborhood of the best solution was then revisited using ellipsoidal shapes in order to check the sensitivity of the solution to the shapes of the components. No significant change of the solution was found for the polar flattening of the primary up to 1.4 and the equatorial elongation of the secondary up to 1.5. We took these values as the upper limits from Naidu et al., 2020 (the 3σ upper limit for the flattening of the primary) and Pravec et al. 2016 (the upper limit for the elongation of the secondary based on statistics of other small binary asteroids), respectively.

The long-period (orbital) lightcurve component data together with the synthetic lightcurve of the best-fit solution are presented in Figs. 2 to 5. A close examination of the figures reveals that while most of the observed events are fitted well, there are some small or moderate discrepancies between the best-fit model and the data in several mutual events. Those include (a) inprecisely modeled shapes of some primary minima, (b) time offsets of some descending or ascending branches of the events or (c) incorrect depths/lengths of some partial events. We ascribe these discrepancies to the model simplifications, namely to the spherical or ellipsoidal approximation of the shape of the primary. Local topography features on the disc (for the case a) or on the limb (for the cases b and c) of the primary are suspected to be causes of the respective effects.

The uncertainty area of the orbital pole is shown in Fig. 6. Figure 7 shows the quadratic drift in the mean anomaly, ΔM, which was computed as follows. We generated a synthetic lightcurve using the model with parameters from the best-fit solution except ΔM_d, which was fixed at zero. Then, for each lightcurve event separately, we fitted the mean anomaly of the model in order to obtain the best match between its synthetic lightcurve and the observed data. ΔM is a difference between the mean anomaly of the original model and the fitted one. For each event, we computed also a standard deviation of ΔM using the procedure described above, but with χ^2 computed only from the data points in the vicinity of the mutual event in question.

3 Parameters of Didymos system

In this section, we summarize the best-fit model parameters of the Didymos binary system that we obtained or took from previous publications. The parameters are listed in Table 2.

In the first part of the table, we present data derived from optical and spectroscopic observations of the system. H_V and G are the mean absolute magnitude and the

Table 2
Parameters of Didymos system

Parameter	Value	Unc.	Reference
Whole system:			
H_V	18.16 ± 0.04	1σ	P12
G	0.20 ± 0.02	1σ	K04
$p_{\rm V}$	0.15 ± 0.04	1σ	N20
Taxon. class	S		C18
Primary:			
$D_{1,\rm V}$ (km)	0.780 ± 0.03	1σ	N20
$D_{1,\rm C}$ (km)	0.786 ± 0.05	1σ	This work / N20[a]
P_1 (h)	2.2600 ± 0.0001	1σ	N20
$(A_1B_1)^{1/2}/C_1$	$1.04^{+0.12}_{-0.04}$	1σ	N20[b]
A_1/B_1	$1.02^{+0.09}_{-0.02}$	1σ	N20[b]
ρ_1 (g cm^{-3})	2.17 ± 0.35	1σ	N20
Secondary:			
$D_{2,\rm C}/D_{1,\rm C}$	0.217 ± 0.004[c]	1σ	This work
$D_{2,\rm C}$ (km)	0.171 ± 0.011	1σ	This work
$D_{2,\rm V}$ (km)	$\geq 0.171 \pm 0.011$	see text	This work
Mutual orbit:			
$a/(A_1B_1)^{1/2}$	$1.59 \pm 0.20/1.51 \pm 0.22$	3σ	This work / N20[d]
a (km)	1.19 ± 0.03	1σ	N20
$L_{\rm P}$ (°)	320.6 ± 13.7[e]	3σ	This work
$B_{\rm P}$ (°)	-78.6 ± 1.8	3σ	This work
ΔM_d (deg/yr^2)	0.15 ± 0.14	3σ	This work
$\dot{n}$ (rad/s^2)	$5.26 \pm 4.91 \times 10^{-18}$	3σ	This work
$P_{\rm orb}$ (h)	11.921624 ± 0.000018[f]	3σ	This work
M_0 (°)	89.1[g]		This work
e	≤ 0.03	3σ	SP09
λ_0 (°)	320.7 ± 9.8[h]	3σ	This work
β_0 (°)	11.5 ± 1.9	3σ	This work
$\lambda_{\rm imp}$ (°)	222.8 ± 7.0[h,i]	3σ	This work
$\beta_{\rm imp}$ (°)	-1.6 ± 4.2	3σ	This work

References: C18: Cheng et al. 2018; K04: Kitazato et al. 2004; N20: Naidu et al. 2020; P06: Pravec et al. 2006; P12: Pravec et al. 2012; SP09: Scheirich and Pravec 2009.
[a] Derived using shape model from N20, see text for details.
[b] Derived using DEEVE from N20, see text for details.
[c] This is a ratio of the cross-section equivalent diameters for the average observed aspect of 9.7°. See text for details.
[d] Derived using DEEVE from N20, see text for details.
[e] For the actual shape of the uncertainty area, see Fig. 6. Semiaxes of the area are 1.8 × 3.0°
[f] The $P_{\rm orb}$, M_0, λ_0 and β_0 values are for epoch JD 2455873.0 (asterocentric UTC, i.e. light-time corrected), for which $P_{\rm orb}$ and ΔM_d do not correlate.
[g] We do not report the uncertainty of M_0, since it is strongly correlated with $L_{\rm P}$. Instead, we report uncertainties of λ_0 and β_0.
[h] For the actual shape of the uncertainty areas of λ_0 vs. β_0 and λ_{imp} vs. β_{imp}, see Fig. 8.
[i] The λ_{imp} and β_{imp} values are for epoch JD 2459849.46875 (2022-09-26.96875) geocentric UTC.

phase parameter of the H–G phase relation (Bowell et al., 1989). $p_{\rm V}$ is the visual geometric albedo derived by Naidu et al. (2020) using H_V and the effective diameter of the whole system from the 3D radar model.

Didymos is classified as an S-type asteroid (Cheng et al., 2018) based on vis-IR spectra obtained by de León et al. (2010).

In the next two parts of Table 2, we give parameters for the components of the binary. The indices 1 and 2 refer to the primary and the secondary, respectively.

$D_{i,\rm C}$ is the mean (rotationally averaged) cross-section equivalent diameter, i.e., the diameter of a sphere with the same cross-section, of the i-th component at the mean aspect of observed total secondary events (see below). To quantify the mean aspect we used an asterocentric latitude of the Phase Angle Bisector (PAB), which is the mean direction between the heliocentric and geocentric directions to the asteroid. As discussed in Harris et al. (1984), this is an approximation for the effective viewing direction of an asteroid observed at the non-zero solar phase. The average absolute value of the asterocentric latitude of the PAB (computed using the nominal pole of the mutual orbit; we assume that the spin poles of both components are the same as the orbit pole) for the observed total events was 9.7°.

$D_{i,\rm V}$ is the volume equivalent diameter, i.e., the diameter of a sphere with the same volume, of the i-th component. $D_{2,\rm C}/D_{1,\rm C}$ is the ratio between the mean cross-section equivalent diameters of the components. P_1 is the rotational period of the primary.

$(A_1B_1)^{1/2}/C_1$ is a ratio between the mean equatorial and the polar axes of the primary. A_1/B_1 is a ratio between the equatorial axes of the primary (equatorial elongation). ρ_1 is the bulk density of the primary.

$D_{1,\rm V}$ and the rotational period of the primary were taken from Naidu et al. (2020). The cross-section equivalent diameter of the primary $D_{1,\rm C}$ was computed from a mean (rotationally averaged) cross-section of the radar shape model from Naidu et al. (2020) at the mean aspect of observed total events (asterocentric latitude of the PAB being 9.7°). We adopted a 6% relative uncertainty for $D_{1,\rm C}$. We note that Naidu et al. (2020) give three uncertainties – 4% for the volume-equivalent diameter of the primary, 6% for the extents along x and y principal axes of the primary, and 10% for the extent along z-axis. The 6% uncertainty appears relevant for our derivation of $D_{1,\rm C}$.

We derived the secondary-to-primary mean cross-section equivalent diameter ratio $D_{2,\rm C}/D_{1,\rm C}$ from the depths of the observed total secondary events. For that, we used the high-quality data for the secondary events observed in November-December 2003, March 2019 and December 2020 (Pravec et al., 2022). The mean depth of the total secondary events was measured to be 0.050 ± 0.002 mag, which gives $D_{2,\rm C}/D_{1,\rm C} = 0.217 \pm 0.004$ (1-σ uncertainties).

From $D_{2,\rm C}/D_{1,\rm C}$ and $D_{1,\rm C}$ we computed $D_{2,\rm C}$. We note that Naidu et al. (2020) reported visible extents of the secondary in the radar data of 150 ± 30 m, which is

consistent with our value.

To calculate the secondary volume equivalent diameter $D_{2,\mathrm{V}}$ from the determined secondary mean cross-section equivalent diameter $D_{2,\mathrm{C}}$, we need to use a shape model for the secondary. As Dimorphos' shape has not been determined yet, we explore a range of possible ellipsoidal shapes for it. For a spherical secondary, we have $D_{2,\mathrm{V}} = D_{2,\mathrm{C}}$. In a case the secondary is a prolate ellipsoid with $A_2/B_2 = 1.5$ and $B_2/C_2 = 1$ —we note that Pravec et al. (2016) found that the equatorial axis ratios of NEA and small MBA binaries show an upper limit of A_2/B_2 about 1.5, hence our choice of the extremally elongated ellipsoid here—, we obtain $D_{2,\mathrm{V}} = 0.173 \pm 0.011$ km. While we see here that the secondary volume equivalent diameter is relatively insensitive to the equatorial axis ratio A_2/B_2, it is more sensitive to B_2/C_2. Unfortunately there is no formal observational or theoretical constraint on the B_2/C_2 for Dimorphos. To show the sensitivity of $D_{2,\mathrm{V}}$ on the polar flattening of the secondary, we calculate $D_{2,\mathrm{V}}$ for an arbitrarily chosen value for B_2/C_2 of 1.5. For a case of the oblate secondary with $A_2/B_2 = 1$ and $B_2/C_2 = 1.5$ we obtain $D_{2,\mathrm{V}} = 0.181 \pm 0.012$ km, while for a case of $A_2/B_2 = 1.5$ and $B_2/C_2 = 1.5$ we obtain $D_{2,\mathrm{V}} = 0.183 \pm 0.012$ km.

Other quantities reported above were taken or derived using data from other sources as we describe in the following.

The mutual orbit and shapes of the Didymos components were modeled by Naidu et al. (2020) from radar observations taken in 2003. They reported the size of the primary to be close to a triaxial ellipsoid with axes 797 × 783 × 761 m (1σ uncertainties of ± 6%, 6% and 10%, respectively). The dimensions given are extents of a dynamically equivalent equal-volume ellipsoid (DEEVE; a homogeneous ellipsoid having the same moments of inertia and volume as the shape model). We used these values to derive $(A_1B_1)^{1/2}/C_1$ and A_1/B_1.

The bulk density of the primary (which they assume is the same as the bulk density of the whole system) was taken from Naidu et al. (2020). For comparison, we derived the bulk density of the whole system from the mutual orbital elements obtained in our work, which leads to 2.44 ± 0.30 g cm^{-3} (1σ).

In the last part of Table 2, we summarize the parameters of the mutual orbit of the binary components. a is the semimajor axis, $L_\mathrm{P}, B_\mathrm{P}$ are the ecliptic coordinates of the orbital pole in the equinox J2000, and M_0 is the mean anomaly of the secondary, measured from the ascending node (as pericenter is not defined for circular orbit) for epoch $t_0 = 2455873.0$ (asterocentric UTC, i.e., light-time corrected). Since M_0 is strongly correlated with L_P, we report only its value for the nominal solution and do not report its uncertainty (which is on the same order as the uncertainty of L_P). Instead, to describe the uncertainty of the position of the secondary in its orbit as an independent parameter, we report its relative ecliptic coordinates with respect to the primary (see below).

e is the orbit eccentricity (only its upper limit is given, reported by Scheirich and Pravec 2009), and ΔM_d is the quadratic drift in the mean anomaly. Since the orbital period P_orb changes with time, the value presented in Table 2 is for the epoch t_0.

For this epoch, which is approximately the mean time of all observed events, a correlation between $P_{\rm orb}$ and ΔM_d is zero. We also give the time derivative of the mean motion $\dot{n}$, derived from ΔM_d.

The uncertainty area of the orbit pole is shown in Fig. 6.

The relative semimajor axis given in Table 2 was derived using the assumption of spherical primary. To test the effect of flattening of the primary on a, we also fitted the data with $(A_1B_1)^{1/2}/C_1$ fixed on three other values: 1.04, 1.16 and 1.40 (these were the nominal value, its 1σ upper limit and 3σ upper limit, respectively, taken from Naidu et al., 2020.). For these three values, we obtained following results for $a/(A_1B_1)^{1/2}$: 1.60 ± 0.20, 1.61 ± 0.20 and 1.63 ± 0.15, respectively.

Naidu et al. (2020) give the value of the mutual semimajor axis to be 1.19 ± 0.03 km (1σ). To compare their result with our value, we computed $a/(A_1B_1)^{1/2}$ using their DEEVE for the primary and their semimajor axis of the mutual orbit. The result is given in Table 2.

λ_0 and β_0 are relative ecliptic coordinates of the secondary with respect to the primary at the epoch t_0. For the nominal time of the DART impact (2022-09-26.96875 geocentric UTC), these coordinates are given by $\lambda_{\rm imp}$ and $\beta_{\rm imp}$.

Note that the uncertainty of $\lambda_{\rm imp}$ is smaller than the uncertainty of λ_0. This is because of following: The time evolution of the uncertainty of λ is governed primarily by two factors: a) at the epochs covered with the data, it is restricted by their amount and quality; b) it grows quadratically into the future from the last apparition. Therefore, the uncertainty is small at the first and the last apparition (panels **a** and **c** on Fig. 8), while at t_0, which is not covered by the data, the uncertianty is larger (panel **b** on Fig. 8). The last panel (**d**) of Fig. 8 shows the uncertainty at the nominal time of the DART impact. To demonstrate the change of the uncertainty more illustratively, we constructed Fig. 9 showing an evolution of the 3-σ uncertainty of λ in time.

4 Mutual events prediction for the 2022–2023 apparition

In order to facilitate planning ground-based observations before and after the DART impact, we computed times of mutual events that will occur in the 2022–2023 apparition using the nominal solution presented in Section 3. It is available at `https://asu.cas.cz/~asteroid/Didymos_2022-2023_events.txt`.

The list includes also the events for a period after the DART impact. Since the prediction in this period is made using the assumption that none of the orbital parameters will change, it has an informative character only.

5 Conclusions

The near-Earth asteroid (65803) Didymos is among the best characterized small asteroid binary systems. It is a typical member of the population of near-Earth asteroid binaries for most of its parameters. With the photometric data taken during five apparitions over time interval of 17 years, we constrained its binary orbit and determined the position of its secondary (Dimorphos) at the time of the DART impact to within $\pm 7.0^\circ$ (3σ uncertainty).

We found that the mean motion of Dimorphos is increasing with a rate of $\dot{n} = 5.26 \pm 4.91 \times 10^{-18}$ rad/s^2 (3σ uncertainty), implying that the mutual semimajor axis is shrinking in time. After the near-Earth binary asteroid (88710) 2001 SL9 (Scheirich et al., 2021), this is the second case with this observed property . As the inward drift of its mutual orbit can not be explined by mutual tides for the system with rotation period of the primary shorter than the orbital period of the secondary, it suggests that the binary YORP (BYORP) effect (McMahon and Scheeres, 2010) acts in the Didymos system.

Acknowledgements

The work was supported by the Grant Agency of the Czech Republic, Grant 20-04431S, and by the project RVO:67985815. Access to computing and storage facilities owned by parties and projects contributing to the National Grid Infrastructure MetaCentrum provided under the program "Projects of Large Research, Development, and Innovations Infrastructures" (CESNET LM2015042), and the CERIT Scientific Cloud LM2015085, is greatly appreciated.

References

Bowell, E., Hapke, B., Domingue, D., Lumme, K., Peltoniemi, J., Harris, A.W., 1989. Application of photometric models to asteroids. In: Asteroids II. Univ. Arizona Press, pp. 524-556.

Cheng, A.F., Rivkin, A.S., Michel, P., Atchison, J., Barnouin, O., Benner, L., Chabot, N.L., Ernst, C., Fahnestock, E.G., Kueppers, M., Pravec, P., Rainey, E., Richardson, D.C., Stickle, A.M., Thomas, C., 2018. AIDA DART asteroid deflection test: planetary defense and science objectives. Planet. Space Sci. 157, 104115.

Dunn, T.L., Burbine, T.H., Bottke, W.F., Jr, Clark, J.P. 2013. Mineralogies and source regions of near-Earth asteroids. Icarus, 222, 273–282.

Harris, A.W., Young, J.W., Scaltriti, F., Zappalà, V., 1984. Lightcurves and phase relations of the Asteroids 82 Alkmene and 444 Gyptis. Icarus 57, 251258.

Kitazato, K., Abe, M., Mito, H., Tarusawa, K., Soyano, T., Nishihara, S., Sarugaku, Y., 2004. Photometric behaviour dependent on solar phase angle and physical characteristics of binary near-Earth Asteroid (65803) 1996 GT. Lunar Planet. Sci. 35.

de León, J., Licandro, J., Serra-Ricart, M., Pinilla-Alonso, N., Campins, H., 2010. Observations compositional, and physical characterization of near-Earth and Marscrosser asteroids from a spectroscopic survey. A&A 517, A23. https://doi.org/10.1051/0004-6361/200913852.

McMahon, J., Scheeres, D., 2010. Secular orbit variation due to solar radiation effects: a detailed model for BYORP. Celest. Mech. Dyn. Astron. 106, 261300.

Michel, P., Kueppers, M., Campo Bagatin, A., et al. 2022. PSJ, submitted.

Naidu, S. P et al. 2020. Radar observations and a physical model of binary near-earth asteroid 65803 Didymos, target of the DART mission, Icarus 348, 113777

Pravec, P., Benner, L. A. M., Nolan, M. C., et al. 2003, IAUC, 8244.

Pravec, P., et al., 2006, Photometric survey of binary near-Earth asteroids, Icarus, 181:6393.

Pravec, P., Harris, A.W., 2007. Binary asteroid population. 1: Angular momentum content. Icarus 190, 250-259.

Pravec, P., et al. 2012. Absolute magnitudes of asteroids and a revision of asteroid albedo estimates from WISE thermal observations, Icarus 221: 365387.

Pravec, P., et al. 2022. Photometric observations of the binary near-Earth asteroid (65803) Didymos in 2015-2021 prior to DART impact. Submitted to Planetary Science Journal.

Rivkin, A. S., Chabot, N. L., Stickle, A. M., et al. 2021, PSJ, 2, 173

Scheirich, P., and Pravec, P., 2009. Modeling of lightcurves of binary asteroids, Icarus, 200:531547.

Scheirich, P. and 36 colleagues, 2021. A satellite orbit drift in binary near-Earth asteroids (66391) 1999 KW4 and (88710) 2001 SL9 - Indication of the BYORP effect, Icarus 360. doi:10.1016/j.icarus.2021.114321

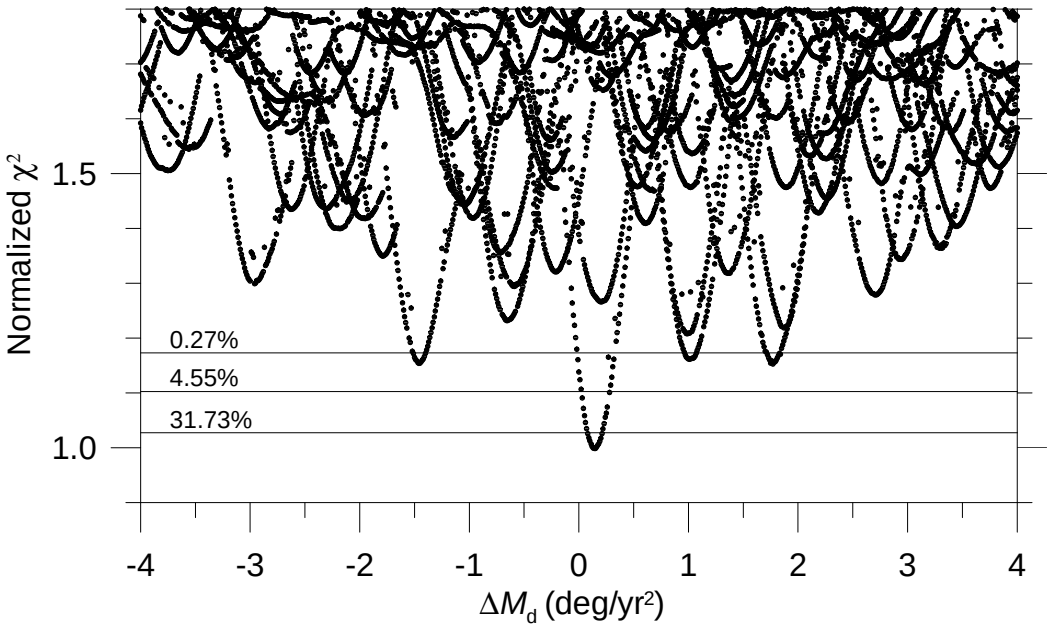

Fig. 1. The normalized χ^2 vs. ΔM_d for solutions of the model presented in Section 2.2. The three horizontal lines give the p-values – the probabilities that the χ^2 exceeds a particular value only by chance, corresponding to 1-, 2- and 3σ interval of the χ^2 distribution with 567 degrees of freedom. See text for details.

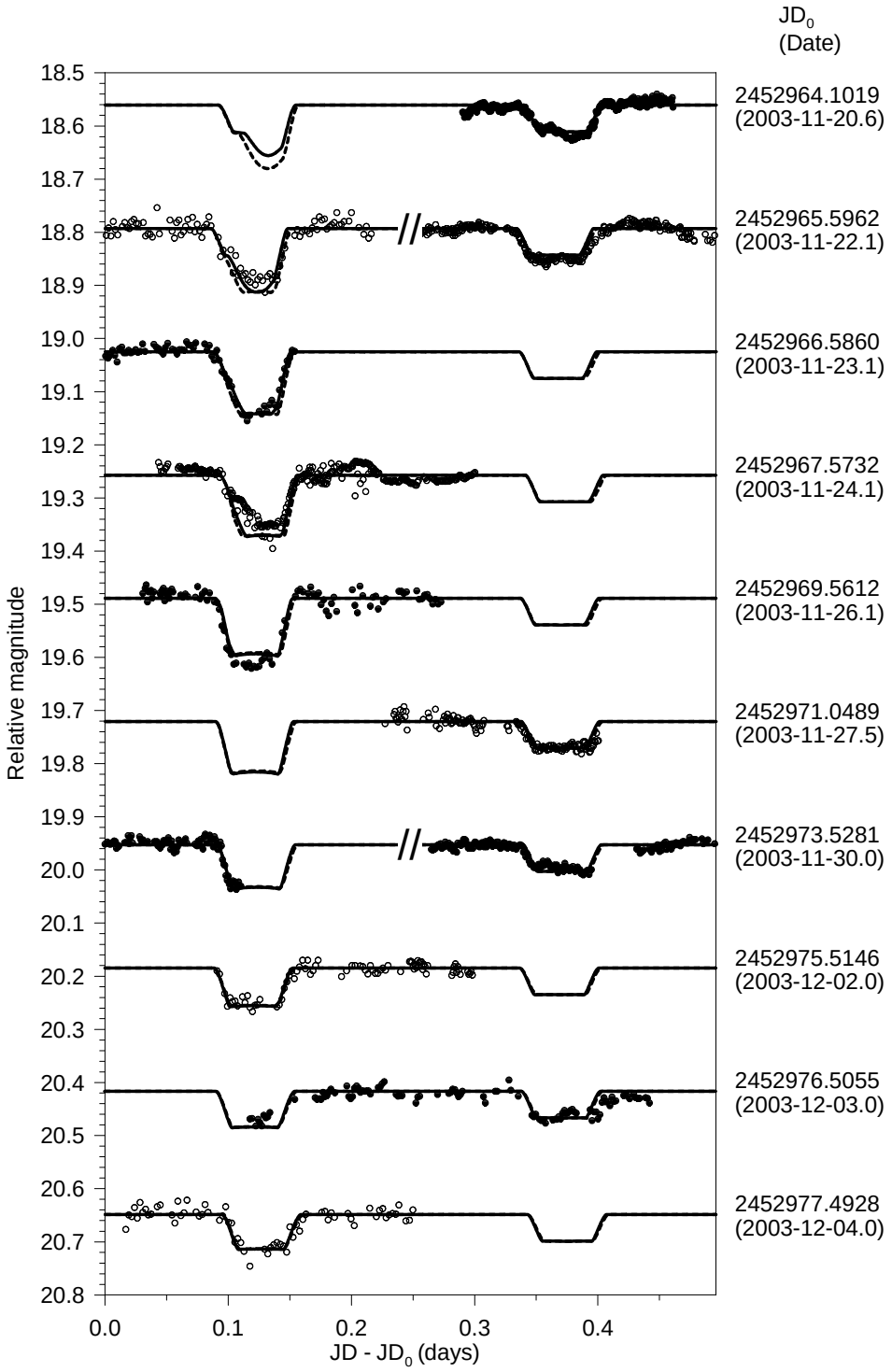

Fig. 2. The orbital lightcurve component of the Didymos system. The observed data are marked as points. The solid curve represents the synthetic lightcurve for the best-fit solution. For comparison, the dashed curve is the model with ΔM_d fixed at 0.0 deg/yr^2 and all other parameters varied to obtain the best fit. The primary and secondary events (the terms refer to which of the two bodies is occulted or eclipsed) are always shown on the left and right side of the plots, respectively. In some cases, the observations of a secondary event precedes that of a primary event (i.e., their order in the dataset is inverse of that shown on the plot). In order to save space in the plot, we present these events in reverse order to how they were observed. They are separated by "//" symbol in the plot and one orbital period (0.496 d) is to be subtracted from x coordinate of data points to the right from this separator.

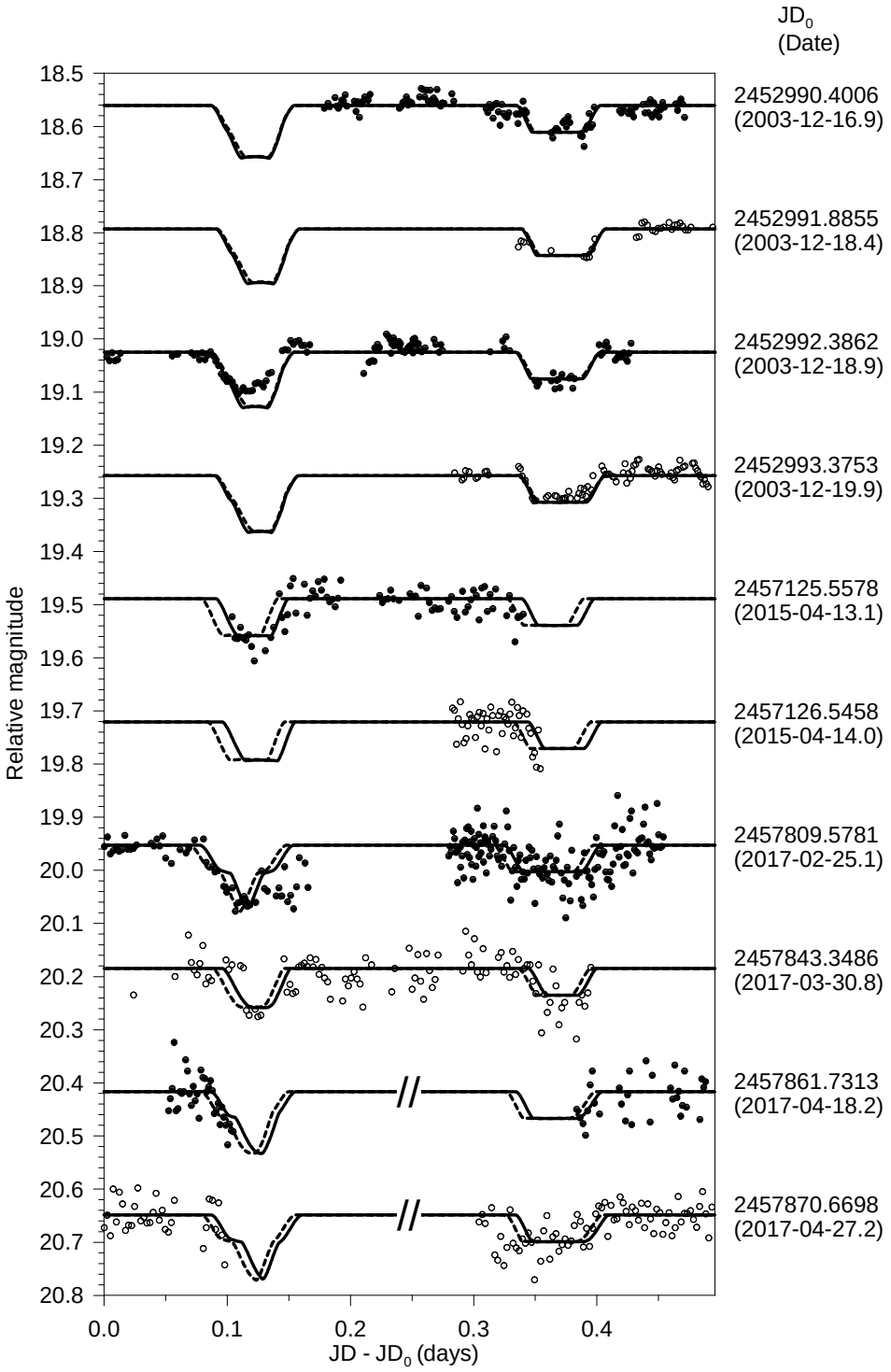

Fig. 3. Continuation of Fig. 2.

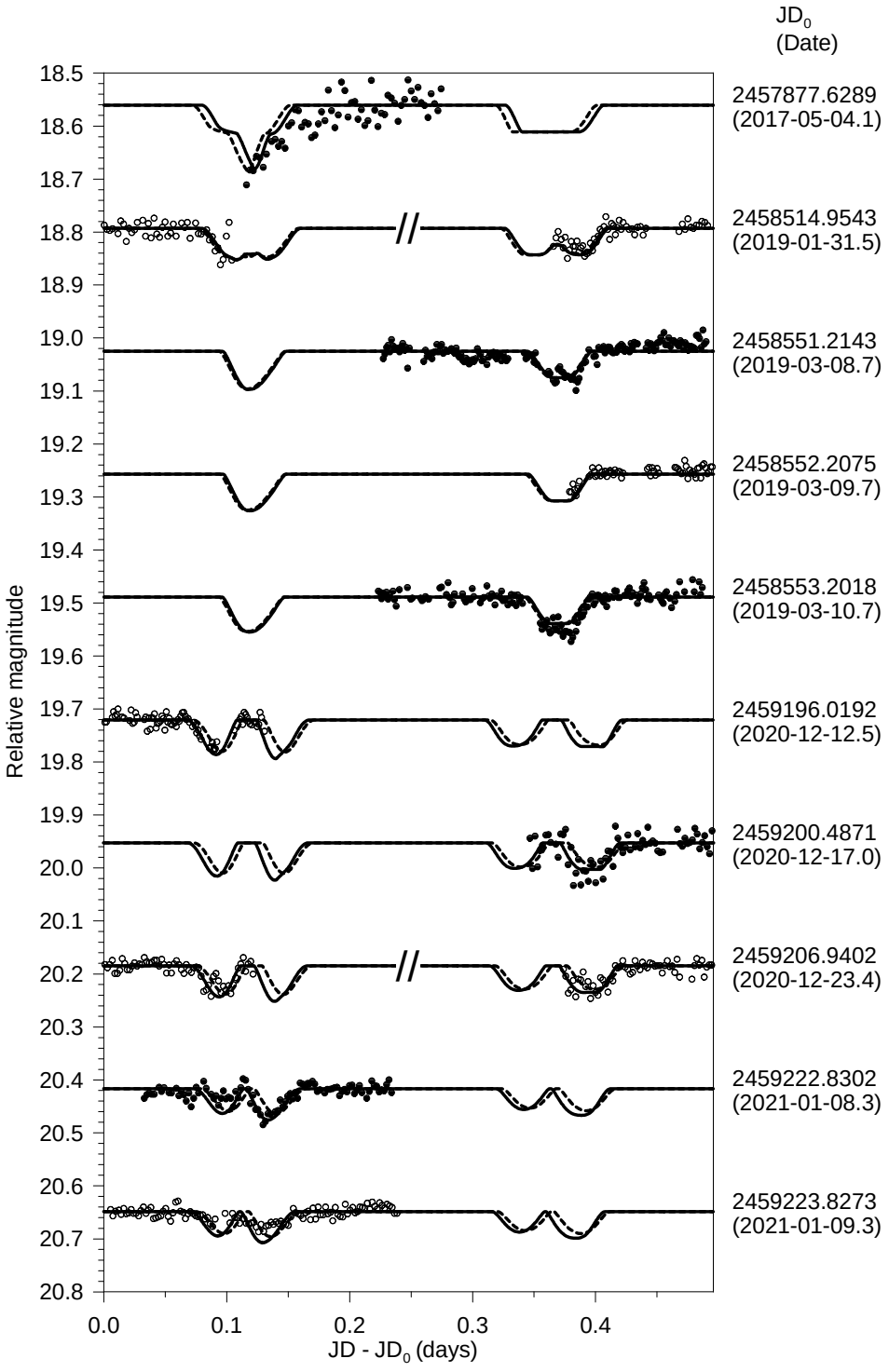

Fig. 4. Continuation of Fig. 2.

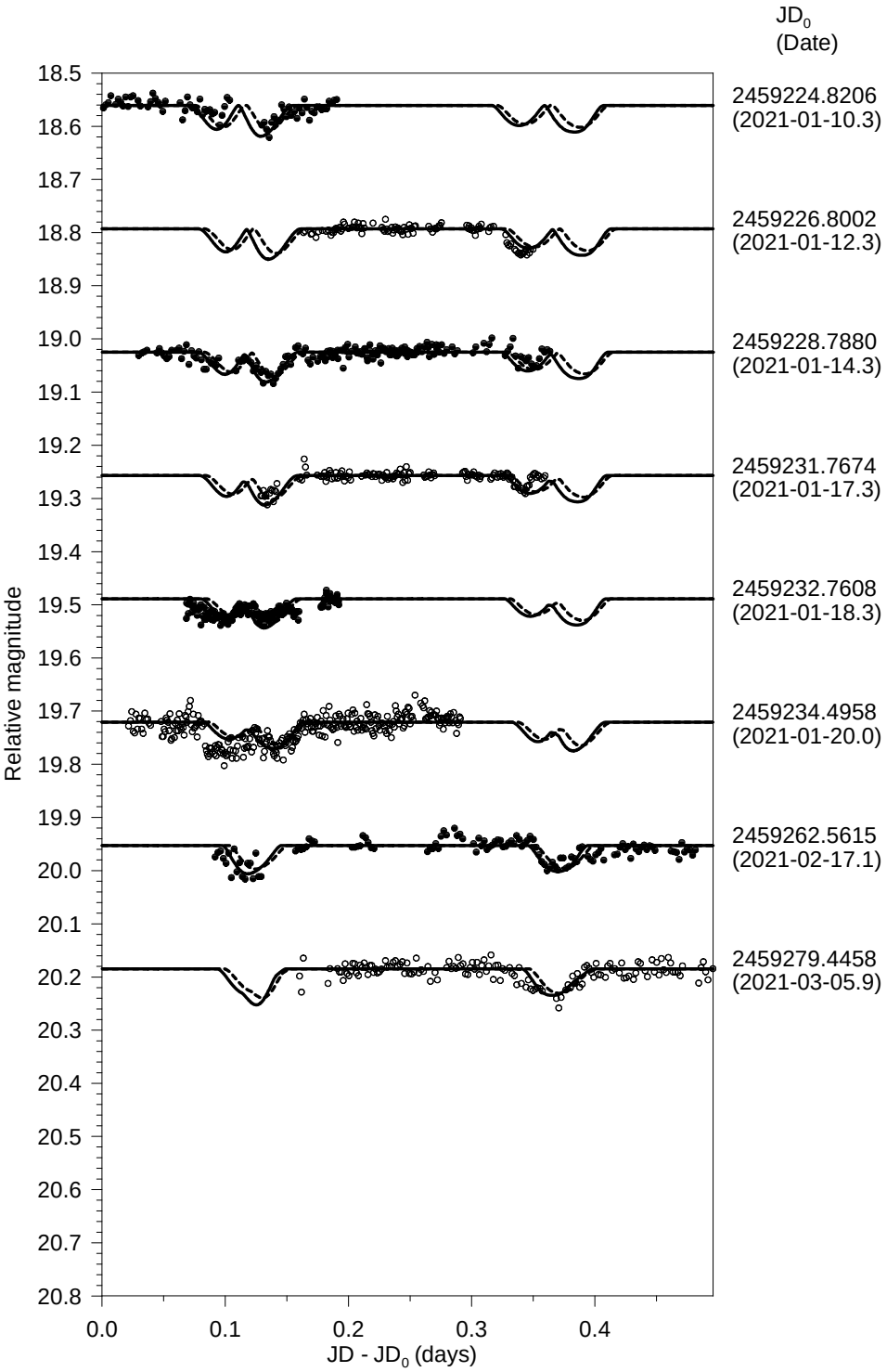

Fig. 5. Continuation of Fig. 2.

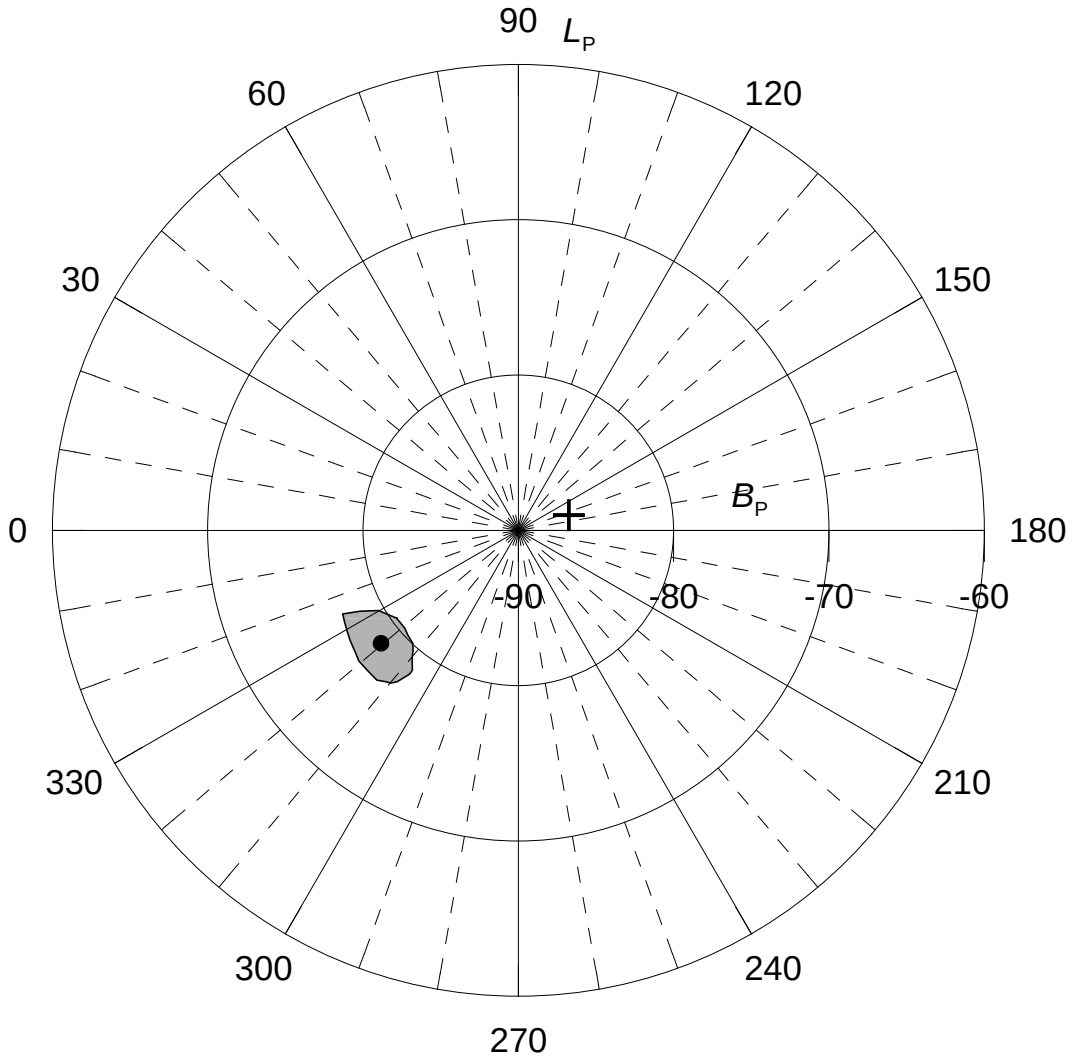

Fig. 6. Area of admissible poles for the mutual orbit of Didymos in ecliptic coordinates (grey area). The dot is the nominal solution given in Table 2. This area corresponds to 3σ confidence level. The south pole of the current asteroid's heliocentric orbit is marked with the cross.

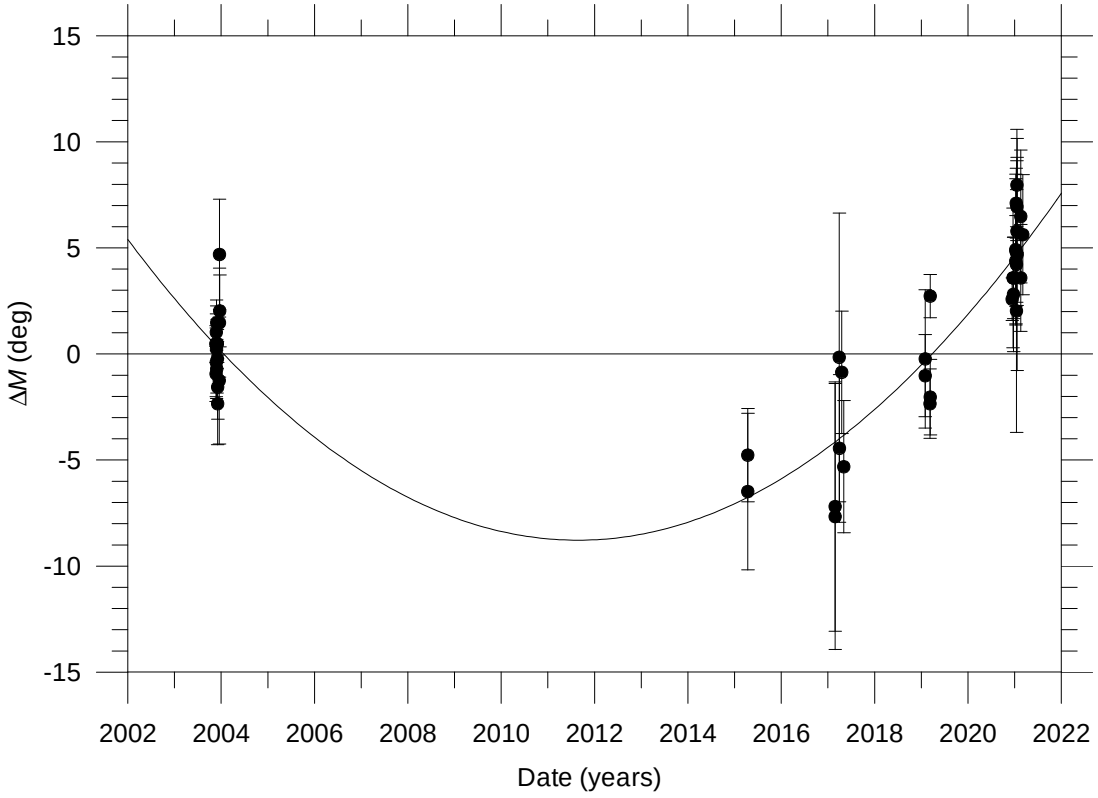

Fig. 7. A time evolution of the mean anomaly difference ΔM with respect to the solution with $\Delta M_d = 0$. See text for details. Each point corresponds to a mutual event covered by the observed data. Vertical error bars represent estimated 1σ uncertainties of the event times, expressed in the mean anomaly. A quadratic fit to the data points, represented by the solid curve, gives the quadratic term of 0.152 deg/yr^2.

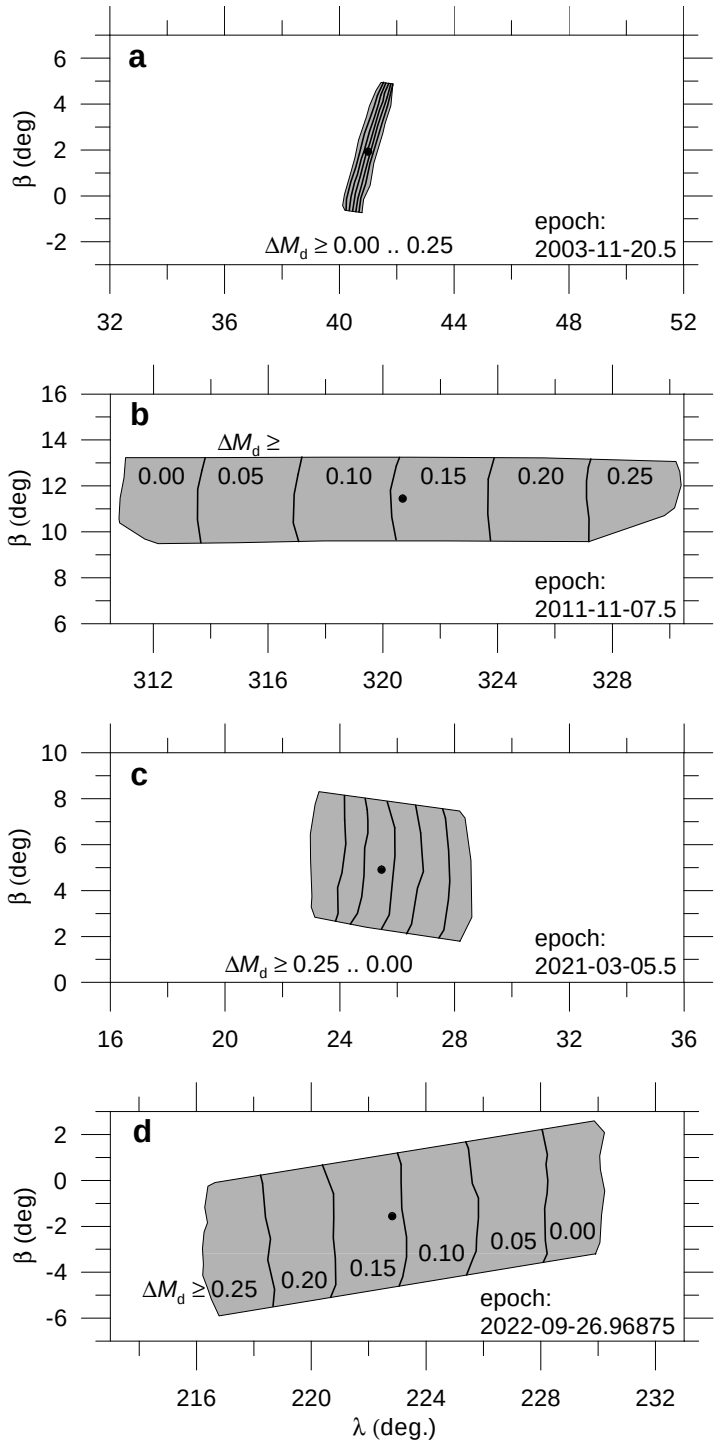

Fig. 8. 3-σ uncertainty area of Dimorphos relative position with respect to Didymos expressed in ecliptical coordinates λ, β (grey areas). To demonstrate the change of size of the uncertainty area with time, we plotted the area for four epochs (2003-11-20.5 – the beginning of the first apparition in 2003; 2011-11-07.5 – epoch JD0; 2021-03-05.5 – the end of the last apparition in 2021; 2022-09-26.96875 – the nominal epoch of the DART impact; panels a, b, c, d, respectively) with the same scale of the axes on all four panels. To show a correlation between λ and ΔM_d, the approximately vertical lines divide areas with $\Delta M_d \geq 0.00; 0.05; 0.10; 0.15; 0.20; 0.25$ deg/yr^2, respectively (the inequality is used becease ΔM_d is correlated with other parameters as well and therefore strict boundaries for its values cannot be given). The dots denote the nominal solution given in Table 2.

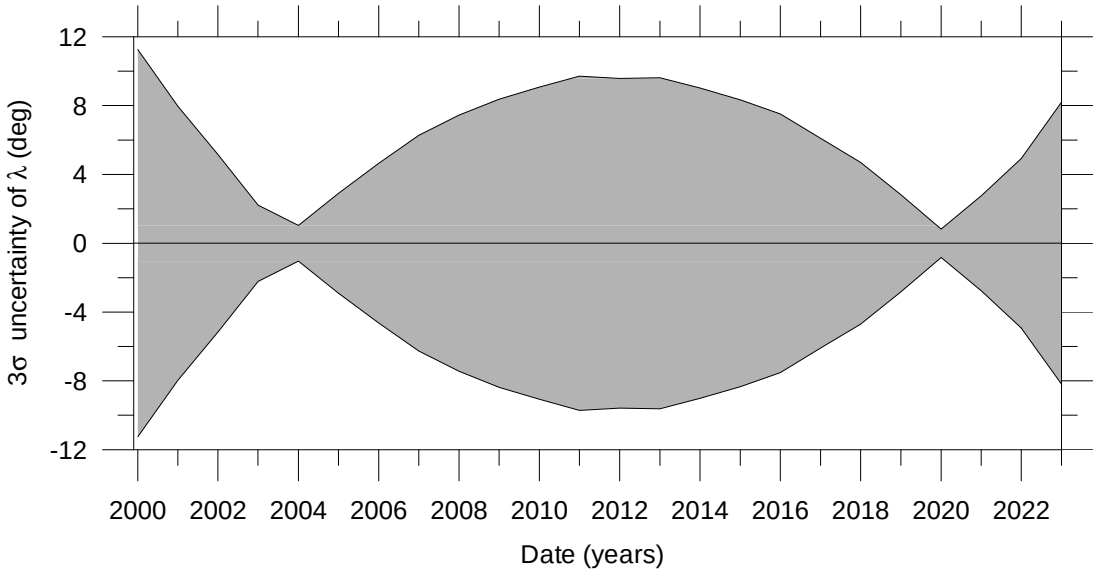

Fig. 9. Evolution of the 3-σ uncertainty of the ecliptic longitude (λ) of the radius vector of Dimorphos with respect to Didymos in time.